Int. J. Heat Mass Transfer. Vol. 36, No. 5, pp. 1315–1331, 1993
Printed in Great Britain

0017-9310/93 $6.00+0.00

Unsteady thermosolutal opposing convection of a liquid–water mixture in a square cavity—I. Flow formation and heat and mass transfer characteristics

J. CHANG, T. F. LIN and C. H. CHIEN
Department of Mechanical Engineering, National Chiao Tung University, Hsinchu, Taiwan, Republic of China

(*Received* 7 *February* 1991 *and in final form* 1 *June* 1992)

Abstract—Transient thermosolutal opposing convection of a liquid–water mixture in a square cavity subject to horizontal temperature and concentration gradients is numerically investigated by a third-order upwind finite-difference scheme. Results are particularly presented to illustrate the effects of the Lewis and Grashof numbers on the evolution of flow patterns and the associated heat and mass transfer characteristics for solutally dominant situations. Results for $Le = 100$ clearly show the double-diffusive nature of the convection. In the initial stage the flow is dominated by the interface velocities at the vertical side walls driven by the concentration gradients there. Later, the flow is governed by the thermal buoyancy. At a much later time, the solutal buoyancy set in inducing new recirculating cells along the side walls. These cells gradually grow and squeeze the thermally driven cell in the core region. Multilayer flow structure is finally formed. The counterrotating cells resulting from the opposing thermal and solutal buoyancies cause significant velocity, temperature and concentration oscillations with time at high Grashof numbers.

1. INTRODUCTION

RECENT interest in the study of thermosolutal convection in cavities has been mainly motivated by its importance in material processing, especially the growth of crystal from melt and vapor. The importance of the convective effects in crystal growing processes by various growth methods was pointed out by Ostrach and his coworkers [1, 2], Langlois [3] and Rosenberger and his group [4–6].

Although cavity flow driven by thermal buoyancy alone has been the focus of many investigations, the thermosolutal convection in cavities has not yet received enough attention. Flow induced by the combined thermal and solutal buoyancies is expected to be much more complex than that in thermal convection. Various modes of flow are possible depending on the relative orientation of the two buoyancy forces, as suggested by Ostrach [7]. In what follows, we confine our attention on thermosolutal convection in cavities with the vertical side walls at different temperatures and concentrations.

To delineate the characteristics of fluid flow and the associated heat and mass transfer, laboratory experiments were recently conducted to directly visualize the cell patterns in thermosolutal convection flows of liquid–water mixture at high Lewis numbers in shallow and tall enclosures subject to the horizontal temperature and concentration gradients by Kamotani *et al.* [8], Ostrach *et al.* [9], Lee and Hyun [10] and Wang *et al.* [11, 12]. Observation of the flow structure was conducted at steady or quasisteady state. Under certain conditions multiple recirculating cells were noted in the flow, forming a layered flow structure. At high thermal and solutal Grashof numbers the flow is unsteady and transitional.

The complex flow characteristics in thermosolutal convection have also received attention from a number of numerical analyses. Ranganathan and Viskanta [13], Han and Kuehn [14], Benard *et al.* [15], Trevisan and Bejan [16] and Hyun and Lee [17, 18] performed numerical calculations to explore the steady features of flow and the associated heat and mass transfer characteristics. Binary gas and liquid mixtures in enclosures with the aspect ratio widely different from unity have been treated. Effects of the Lewis number and buoyancy ratio were investigated. Lewis number was found to have an important bearing on the flow pattern. Multiple cellular flow was predicted by Han and Kuehn [14] at the Lewis number of 250. Oscillatory flow and thermosolutal characteristics were considered by Krishnan [19] in a square enclosure with the Prandtl and Schmidt numbers chosen as 1 and 3.162, respectively. The thermal and solutal buoyancies oppose each other but with equal strength. As the Rayleigh number is over 6.25×10^4, successive bifurcations to oscillatory flow motion are noted. The flow follows a quasiperiodic route to chaos.

Scale analysis of the problem for the limiting cases of heat transfer driven and mass transfer driven situations in the boundary layer regime covering wide ranges of the Prandtl and Schmidt numbers was carried out by Bejan [20]. Based on their experimental observation for opposing flow, Jiang *et al.* [21] sug-

NOMENCLATURE

D solutal diffusivity
g gravitational acceleration
Gr_t, Gr_s Grashof numbers of heat and mass transfer
H height of enclosure
N buoyancy ratio
Nu_x, $\overline{Nu}$ local and average Nusselt numbers
n time step
P, p_d dimensionless and dynamic pressures
Pr, Sc Prandtl and Schmidt numbers
Ra_t, Ra_s thermal and solutal Rayleigh numbers
Sh_x, $\overline{Sh}$ local and average Sherwood numbers
t, τ dimensional and dimensionless time
T^0, T dimensional and dimensionless temperatures
T_H^0, T_C^0 hot and cold wall temperatures
u, v vertical and horizontal velocity components
U, V dimensionless vertical and horizontal velocity components
W_{1i}^0, W dimensional and dimensionless mass fractions of species 1
W_{1H}^0, W_{1L}^0 high and low mass fractions of species 1.

Greek symbols
α thermal diffusivity of the mixture
β_t, β_s thermal and solutal volumetric expansion coefficients
δ_t, δ_s thermal and solutal boundary layer thickness
ΔT^0, ΔW_1^0 temperature and concentration differences, $(T_H^0 - T_C^0)$ and $(W_{1H}^0 - W_{1L}^0)$
Γ concentration ratio
ν kinematic viscosity of the mixture
ξ, η transformed coordinates for X and Y
ρ mass density of the mixture.

Subscripts
i,j node indices
x, y x- and y-directions.

gested three possible flow patterns in a low aspect ratio enclosure. Depending on the magnitude of the buoyancy ratio, the flow may appear as multilayer, secondary flow or mixed flow.

The literature just reviewed clearly indicates that the flow and heat and mass transfer characteristics are significantly affected by all the governing non-dimensional groups—the Prandtl number, Lewis number, thermal Grashof number, buoyancy ratio, aspect ratio, and the interface velocities at the side walls. Although the cell patterns at steady or statistical state have been reported, the processes of the cell formation evolved from the initially quiescent state remain unknown. Moreover, the details of the transport processes in the fluctuating flow resulting from high thermal and solutal buoyancies are still not fully understood. In an initial attempt to explore the detailed mechanisms of momentum, energy and species transfer in the thermosolutal convection in enclosure, Lin *et al.* [22] carried out a detailed numerical computation to simulate the temporal evolution of the velocity, temperature and concentration fields in a square enclosure containing binary gas mixture subject to horizontal temperature and concentration gradients.

In this study, we extend the above analysis [22] to unravel the detailed momentum, heat and mass transfer mechanisms in a buoyancy driven binary mixture of liquid–water in a square enclosure. Since Le is much greater than unity in the liquid mixture, thermal diffusion proceeds at a much higher speed than that of species diffusion and the thermal boundary layer is much thicker than the solutal boundary layer [9] with $\delta_t/\delta_s = (Le \cdot |N|)^{1/4}$. These unique features are expected to result in complex flow patterns especially in buoyancy opposing flows. Time-dependent numerical simulation for two-dimensional opposing double-diffusive natural convection in a square enclosure is performed here with the Prandtl number fixed at 7.6, Lewis number varied from 10 to 100, thermal Grashof number from 10^3 to 2×10^5, buoyancy ratio from -5 to -15, and interface velocity parameter from 10 to 50. Although the thermosolutal convection can be three-dimensional under certain conditions [21], in this initial attempt a two-dimensional model is used to facilitate the analysis. The use of a two-dimensional model to predict three-dimensional thermal convection cavity flow in the unsteady and transitional regimes was found to be satisfactory by Schladow *et al.* [23] and Paolucci and Chenoweth [24]. The results obtained from this study are presented in the present article and the one that follows. This article concentrates on the effects of the governing non-dimensional parameters on the processes of the cell formation and the associated heat and mass transfer characteristics. In Part II we focus on the bifurcation leading to the oscillatory flow motion at high Rayleigh numbers. Results from power spectrum analysis will be given to elucidate the fluctuating characteristics.

2. MATHEMATICAL FORMULATION

Under consideration is a binary liquid mixture confined in a square enclosure with its depth much larger than its height and width so that the flow can be treated as two dimensional. The top and bottom boundaries of the enclosure are thermally well insulated and impermeable. Initially, the stationary liquid and confining walls are assumed to be at the same uniform temperature T_i^0 and same uniform concentration W_{1i}^0. At $t = 0$, the temperatures at right and left vertical walls are suddenly raised to a higher level $T_i^0 + \Delta T^0/2$ and lowered to a lower level $T_i^0 - \Delta T^0/2$, respectively, and maintained at these levels thereafter. Meanwhile, the concentrations of the fluid at the left and right vertical walls are hypothesized to be abruptly elevated to a higher value $W_{1i}^0 + \Delta W_1^0/2$ and dropped to a lower value $W_{1i}^0 - \Delta W_1^0/2$, respectively. For the buoyancy opposing flow considered the left wall is maintained at a higher concentration, while the right wall is at a lower concentration. Accordingly, horizontal temperature and concentration gradients are imposed on the fluid, and the flow is then initiated and evolves under the action of the combined driving forces due to these gradients. The transient developments of flow, temperature and concentration fields in the cavity can be predicted, with the Boussinesq approximations [7, 13, 25], by solving the following nondimensional governing differential equations.

Continuity equation:

$$\frac{\partial U}{\partial X} + \frac{\partial V}{\partial Y} = 0. \tag{1}$$

X-direction momentum equation:

$$\frac{\partial U}{\partial \tau} + U\frac{\partial U}{\partial X} + V\frac{\partial U}{\partial Y} = -\frac{\partial P}{\partial X} + Pr\left(\frac{\partial^2 U}{\partial X^2} + \frac{\partial^2 U}{\partial Y^2}\right) + Gr_t Pr^2 (T + NW). \tag{2}$$

Y-direction momentum equation:

$$\frac{\partial V}{\partial \tau} + U\frac{\partial V}{\partial X} + V\frac{\partial V}{\partial Y} = -\frac{\partial P}{\partial Y} + Pr\left(\frac{\partial^2 V}{\partial X^2} + \frac{\partial^2 V}{\partial Y^2}\right). \tag{3}$$

Energy equation:

$$\frac{\partial T}{\partial \tau} + U\frac{\partial T}{\partial X} + V\frac{\partial T}{\partial Y} = \frac{\partial^2 T}{\partial X^2} + \frac{\partial^2 T}{\partial Y^2}. \tag{4}$$

Species diffusion equation:

$$\frac{\partial W}{\partial \tau} + U\frac{\partial W}{\partial X} + V\frac{\partial W}{\partial Y} = \left(\frac{\partial^2 W}{\partial X^2} + \frac{\partial^2 W}{\partial Y^2}\right)\Big/ Le. \tag{5}$$

In writing the above equations the following nondimensional variables were introduced:

$$X = x/H, \quad Y = y/H, \quad U = u/(\alpha/H)$$
$$V = v/(\alpha/H), \quad P = p_d/(\rho\alpha^2/H^2), \quad \tau = t/(H^2/\alpha)$$
$$Pr = \nu/\alpha, \quad T = (T^0 - T_i^0)/\Delta T^0, \quad Sc = \nu/D$$
$$W = (W_1^0 - W_{1i}^0)/\Delta W_1^0, \quad Le = Sc/Pr = \alpha/D$$
$$N = \beta_s \cdot \Delta W_1^0/\beta_t \cdot \Delta T^0, \quad Gr_t = g\beta_t H^3 \cdot \Delta T^0/\nu^2$$
$$Gr_s = g\beta_s H^3 \cdot \Delta W_1^0/\nu^2. \tag{6}$$

The initial and boundary conditions for the flow are

when $\tau \leqslant 0$:

$$U = V = P = 0, \quad T = W = 0 \tag{7a}$$

when $\tau > 0$:

at

$$Y = 0, \quad T = -0.5; \quad W = -0.5;$$
$$V = -\frac{1}{Le}\cdot\frac{1}{\Gamma}\cdot\frac{\partial W}{\partial Y}; \quad U = 0, \tag{7b}$$

at

$$Y = 1, \quad T = 0.5; \quad W = 0.5;$$
$$V = -\frac{1}{Le}\cdot\frac{1}{\Gamma - 1}\cdot\frac{\partial W}{\partial Y}; \quad U = 0, \tag{7c}$$

at

$$X = 0 \text{ and } 1, \quad \frac{\partial T}{\partial X} = \frac{\partial W}{\partial X} = U = V = 0. \tag{7d}$$

The interface velocities of the binary mixture induced by the mass diffusion at the side walls are specified in equations (7b) and (7c) with $\Gamma = (1 - W_{1L}^0)/(W_{1H}^0 - W_{1L}^0)$. It is relatively important during the early transient period [26].

It is noticed that the volumetric expansion coefficient due to temperature change, defined as $\beta_t = -(1/\rho)(\partial\rho/\partial T^0)_{W_{1,p}^0}$, is normally positive, but the volumetric expansion coefficient for concentration change, defined as $\beta_s = -(1/\rho)(\partial\rho/\partial W_1^0)_{T_{1,p}^0}$ can be either positive or negative. In this study β_s is taken to be negative, that is, component 1 is assumed to be heavier than component 2 in the mixture $(\partial\rho/\partial W_1^0 > 0)$. As a result, the buoyancy ratio N is always negative. To facilitate the analysis, the thermophysical properties of the mixture are considered to be constant except the density in the buoyancy terms [7, 13]. This simplification is appropriate when both components in the mixture have comparable molecular weights or when the mixture is dilute [27].

The transient local Nusselt and Sherwood numbers on the vertical walls can be evaluated by these equations

$$Nu_x = \begin{cases} (\partial T/\partial Y)_{Y=0} & \text{for right wall} \\ (\partial T/\partial Y)_{Y=1} & \text{for left wall} \end{cases} \tag{8}$$

and

$$Sh_x = \begin{cases} (\partial W/\partial Y)_{Y=0} & \text{for right wall} \\ (\partial W/\partial Y)_{Y=1} & \text{for left wall} \end{cases}. \tag{9}$$

Integrating the results for local Nusselt and Sherwood numbers along a given wall yields the results for the average Nusselt and Sherwood numbers for that wall. For instance, at the right wall

$$\overline{Nu} = \int_0^1 [(\partial T/\partial X)_{Y=0}]\, \mathrm{d}Y \tag{10}$$

and

$$\overline{Sh} = \int_0^1 [(\partial W/\partial X)_{Y=0}]\, \mathrm{d}Y. \tag{11}$$

3. SOLUTION METHOD

Since the flow governed by equations (1)–(5) is known to be parabolic in time but elliptic in space, the solution for the problem can only be marched in time, and iterative procedures must be employed to obtain the solution in the spatial domain. The projection method developed by Chorin [28] and Temam [29] was chosen to numerically solve the time-dependent governing equations in their primitive form with three interlacing staggered grids, respectively, for the horizontal velocity component, vertical velocity component, and all scalar variables. This fractional-step method consists of two steps. First, a provisional value is explicitly computed for velocity field ignoring the pressure gradient such as

$$\frac{\mathbf{V}^* - \mathbf{V}^n}{\Delta\tau} + A(\mathbf{V}^n) - \frac{1}{Re}\cdot\nabla^2\mathbf{V}^n = 0 \tag{12}$$

where $A(\mathbf{V}^n)$ is the convection term, $A(\mathbf{V}^n) = (\mathbf{V}\cdot\nabla)\mathbf{V}$. Then, the provisional velocity field $\mathbf{V}^*$ is corrected by including the pressure effect and by enforcing the mass conservation at time step $n+1$,

$$\frac{\mathbf{V}^{n+1} - \mathbf{V}^*}{\Delta\tau} + \nabla P^{n+1} = 0 \tag{13}$$

and

$$\nabla\cdot\mathbf{V}^{n+1} = 0. \tag{14}$$

Substituting equation (14) into equation (13) yields the Poisson equation for pressure,

$$\nabla^2 P^{n+1} = \frac{1}{\Delta\tau}\nabla\cdot\mathbf{V}^*. \tag{15}$$

In discretizing the above equations, centered difference is used to approximate all the derivatives except the convective terms. To enhance numerical stability and to yield accurate results, a third-order upwind scheme developed by Kawamura *et al.* [30] is

Table 1. Comparison with the solution from different authors for the limiting case of $Pr = 0.71$, $Ra_t = 10^6$

	$\lvert\psi\rvert_{max}$ X, Y	V_{max} Y	U_{max} X	Nu_0	Nu_{min} X	Nu_{max} X
Bench mark solution†	16.75 0.547, 0.151	64.63 0.850	219.36 0.0379	8.817	0.989 1.0	17.925 0.0378
'Exact' solution‡	—	64.91 0.849	220.80 0.0381	8.822	—	—
41×41¶ $\beta_x = 1.10$ $\beta_y = 1.10$	16.82 0.553, 0.155	64.74 0.871	221.06 0.0421	8.857	0.9510 0.9962	18.112 0.0376
41×41¶ $\beta_x = 1.03$ $\beta_y = 1.03$	16.758 0.554, 0.146	64.21 0.854	219.52 0.0323	8.811	0.9731 0.9983	17.901 0.0164
41×41¶ $\beta_x = 1.06$ $\beta_y = 1.06$	16.757 0.541, 0.152	64.35 0.863	220.17 0.0365	8.830	0.9659 0.9911	17.811 0.0345
51×51¶ $\beta_x = 1.06$ $\beta_y = 1.06$	16.765 0.543, 0.152	64.45 0.856	220.65 0.0422	8.828	0.9674 0.9931	17.704 0.0423
61×61¶ $\beta_x = 1.06$ $\beta_y = 1.08$	16.760 0.546, 0.149	64.65 0.854	220.38 0.0398	8.825	0.9876 0.9971	17.661 0.0382

$\lvert\psi\rvert_{max}$ the maximum absolute value of the stream function (together with its location, X, Y);
U_{max} the maximum vertical velocity on the vertical mid-plane of the cavity (together with its location, X);
V_{max} the maximum vertical velocity on the horizontal mid-plane of the cavity (together with its location, Y);
Nu_0 the average Nusselt number on the vertical boundary at $X = 0$;
Nu_{max} the maximum value of the local Nusselt number on the boundary at $X = 0$ (together with its location, Y);
Nu_{min} the minimum value of the local Nusselt number on the boundary at $X = 0$ (together with its location, Y).

† Bench mark solution from de Vahl Davis [34].
‡ 'Exact' solution from Chenoweth and Paolucci [35].
¶ Present solution.

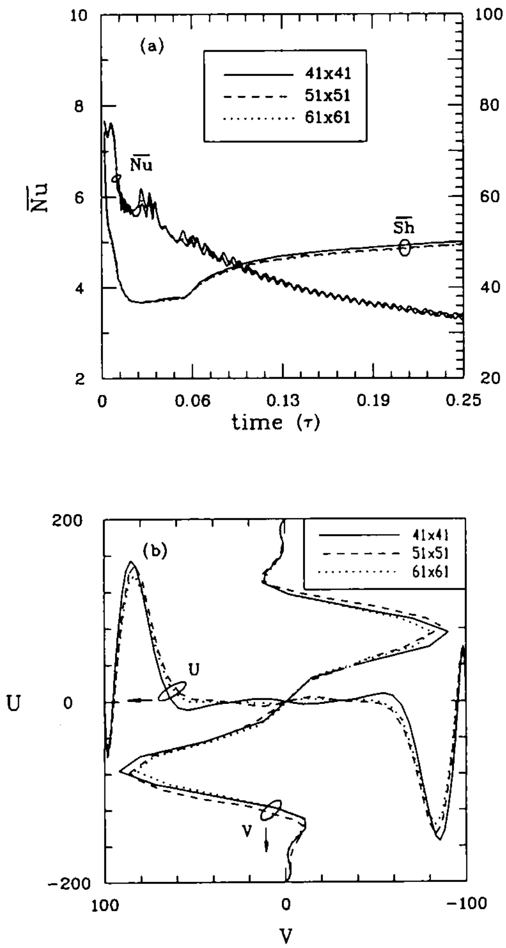

FIG. 1. Grid-independence tests for (a) time series of the average Nusselt and Sherwood numbers and (b) U and V profiles at their respective mid-planes at $\tau = 0.25$ for the thermosolutal cavity convection with $Pr = 7.6$, $Le = 100$, $Gr_t = 2\times 10^5$, $N = -5$ and $\Gamma = 50$.

employed to discretize these convective terms. For instance, in the X-direction momentum equation

$$\left(U\frac{\partial U}{\partial X}\right)_{i,j} = U_{i,j}(U_{i+2,j}-2U_{i+1,j}+9U_{i,j}-10U_{i-1,j}+2U_{i-2,j})/6\Delta X,\quad \text{for}\quad U_{i,j}\geqslant 0$$

or

$$U_{i,j}(-2U_{i+2,j}+10U_{i+1,j}-9U_{i,j}+2U_{i-1,j}-U_{i-2,j})/6\Delta X,\quad \text{for}\quad U_{i,j}<0. \quad (16)$$

In order to accurately resolve the steep velocity, temperature and concentration gradients in the wall boundary layers at high thermal and solutal Rayleigh numbers, a nonuniform grid system is required. Instead of employing the nonuniform grid directly, we transformed the nonuniform ΔX_i and ΔY_j in the finite difference equations into a uniform grid using orthogonal transformation along two coordinates with the same transformation function [31]

$$\xi = 1/2+1/2\cdot\ln[(\beta_x+2X-1)/(\beta_x+2X+1)]/\ln[(\beta_x+1)/(\beta_x-1)] \quad (17a)$$

$$\eta = 1/2+1/2\cdot\ln[(\beta_y+2Y-1)/(\beta_y-2Y+1)]/\ln[(\beta_y+1)/(\beta_y-1)] \quad (17b)$$

where β_x and β_y are stretching parameters for adjusting the grid nonuniformity. To further improve the numerical simulation, we adopted the following centered finite-difference representation for the first and second derivatives developed by Kálnay de Rivas [32].

$$\left(\frac{\partial f}{\partial X}\right)_i = \frac{f_{i+1}-f_{i-1}}{2\Delta\xi(\mathrm{d}X/\mathrm{d}\xi)_i(1+1/6\cdot\delta_{i,x})} \quad (18a)$$

$$\left(\frac{\partial^2 f}{\partial X^2}\right)_i = \frac{(f_{i+1}-f_i)\bigg/\left(\frac{\mathrm{d}X}{\mathrm{d}\xi}\right)_{i+1/2}-(f_i-f_{i-1})\bigg/\left(\frac{\mathrm{d}X}{\mathrm{d}\xi}\right)_{i-1/2}}{(\Delta\xi)^2(\mathrm{d}X/\mathrm{d}\xi)_i(1+5/24\cdot\delta_{i,x})} \quad (18b)$$

where $\delta_{i,x} = (\Delta\xi)^2(\mathrm{d}^3X/\mathrm{d}\xi^3)_i/(\mathrm{d}X/\mathrm{d}\xi)$. These approximations are particularly useful when large grid variation is used. The above approximation has a truncation error of $O(\Delta\xi^2)$ for arbitrary mesh transformation in problems of boundary layer character. The same procedure may be done along the Y-coordinate. For the convection terms, the improved centered difference in equation (18a) is only applied to the boundary nodes in normal direction where the velocity is low due to the presence of the solid boundaries. These improved finite-difference approximations, equations (18a) and (18b), combining with the third-order upwind convective scheme, equation (16), for the interior nodes yield very accurate results.

Time advancement may be done either implicitly or explicitly. The first-order Euler explicit scheme was employed since it was easy to implement. It has a much lower computational cost per timestep, and requires much less computer memory allocation than any equivalent implicit implementation. We also found that the first-order scheme was sufficiently accurate to resolve the smallest physical timescale. The stability of the scheme limited by the requirement that the Courant number be less than unity [31] was found to be governed by the smallest grid spacing normal to the confining walls. The timestep selected to comply with the above stability limitation was smaller than that required to resolve the largest frequency that appears in the flow considered.

The sequence of numerical operation is as follows:

(1) explicitly calculate $\mathbf{V}^*$ from equation (12),
(2) solve the pressure equation for P^{n+1} by the modified strong implicit procedure (MSIP) method developed by Schneider and Zedan [33],
(3) explicitly calculate the desired velocity field at the new time step, $\mathbf{V}^{n+1}$, from equation (13).

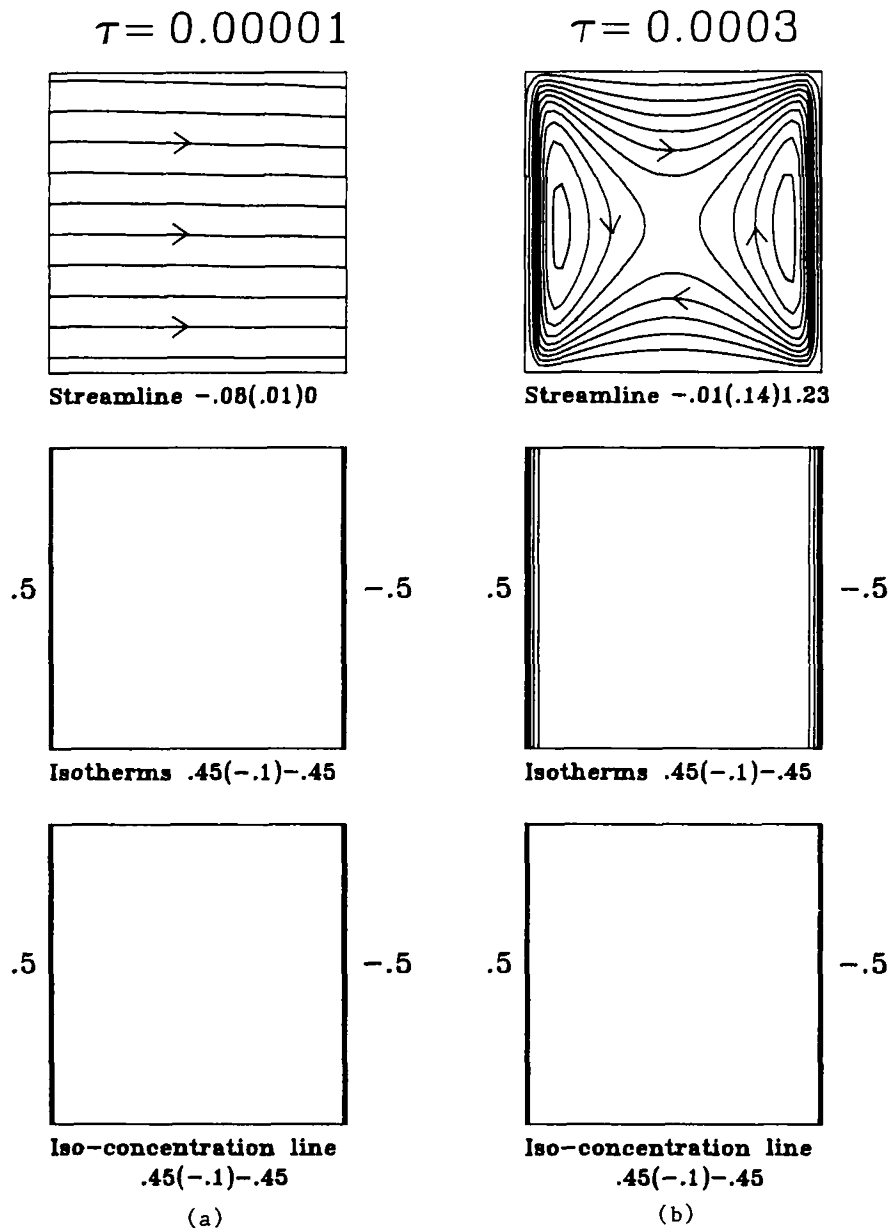

FIG. 2. Time evolution of flow patterns, isotherms and iso-concentration lines for opposing flow for $Pr = 7.6$, $Le = 10$, $Gr_t = 10^5$, $N = -5$ and $\Gamma = 50$ at (a) $\tau = 0.00001$, (b) $\tau = 0.0003$, (c) $\tau = 0.003$, (d) $\tau = 0.01$, (e) $\tau = 0.05$, (f) $\tau = 0.08$.

The energy and species diffusion equations were solved by the simple explicit method.

To verify the proposed numerical algorithm, a series of stringent numerical tests were performed to ensure the solutions were accurate and grid-independent. First, the present numerical algorithm was applied to the limited cases of pure thermal convection of air in a square enclosure. Results computed by 41×41, 51×51 and 61×61 grids with different β_x and β_y for a typical case of $Pr = 0.71$ and $Ra_t = 10^6$ are compared with the steady state benchmark solution of de Vahl Davis [34] and the 'Exact solution' of Chenoweth and Paolucci [35] in Table 1. Excellent agreement is observed. Next, the predicted transient pure thermal convection ($N = 0$) in a square cavity at very high Rayleigh numbers is compared with the experimental and numerical results of Patterson and Armfield [36] and Schladow *et al.* [23]. Our predicted temperature variation with time at a location inside the wall boundary layer for $Pr = 7.5$ and $Ra_t = 3.26 \times 10^8$ is in good agreement with the measured data. Moreover, the vertical velocity and temperature profiles at 20 s after the initiation of the transient at the midheight of the cavity for $Ra_t = 2 \times 10^9$ computed from the present

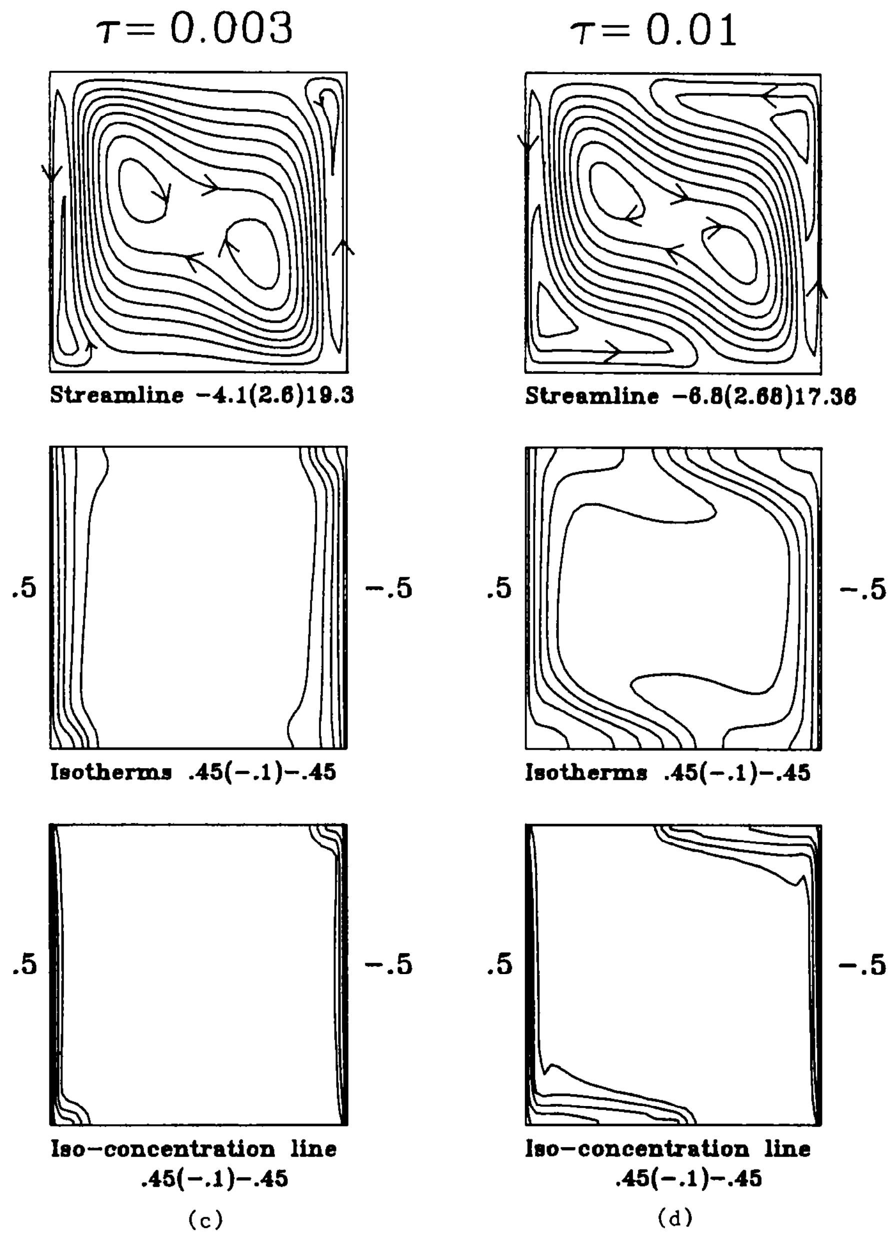

FIG. 2—*Continued.*

method with the 61×61 grid agree excellently with those predicted from the second-order quadratic upwind scheme (QUICK) by Schladow *et al.* [23] with the 90×90 grid. Then, the temporal variations of the calculated average Nusselt and Sherwood numbers along with the vertical and horizontal velocity profiles at $x = 0.5$ and $y = 0.5$ at $\tau = 0.25$ from three different grids for a typical case of thermosolutal convection with $Pr = 7.6$, $Le = 100$, $Gr_t = 2 \times 10^5$, $N = -5$, $\Gamma = 50$ are shown in Fig. 1. Good agreement is again noted by contrasting the predictions from those grids. It is recognized, however, that some phase error does exist in numerically calculating the transient oscillatory flow (Fig. 1(a)). But, this phase error is not expected to significantly affect the essential characteristics of the flow at large τ, such as the amplitude and frequencies of the oscillations. Finally, results from the time-interval test are examined. Halving the time interval from 10^{-6} to 5×10^{-7} is found to cause unnoticeable changes in the results. Through these program tests, the 41×41 grid with $\beta_x = \beta_y = 1.06$ and $\Delta\tau = 10^{-6}$ is considered to be good enough for numerically exploring the major characteristics of the transient buoyancy induced flow and heat and mass transfer in a square enclosure to be studied here.

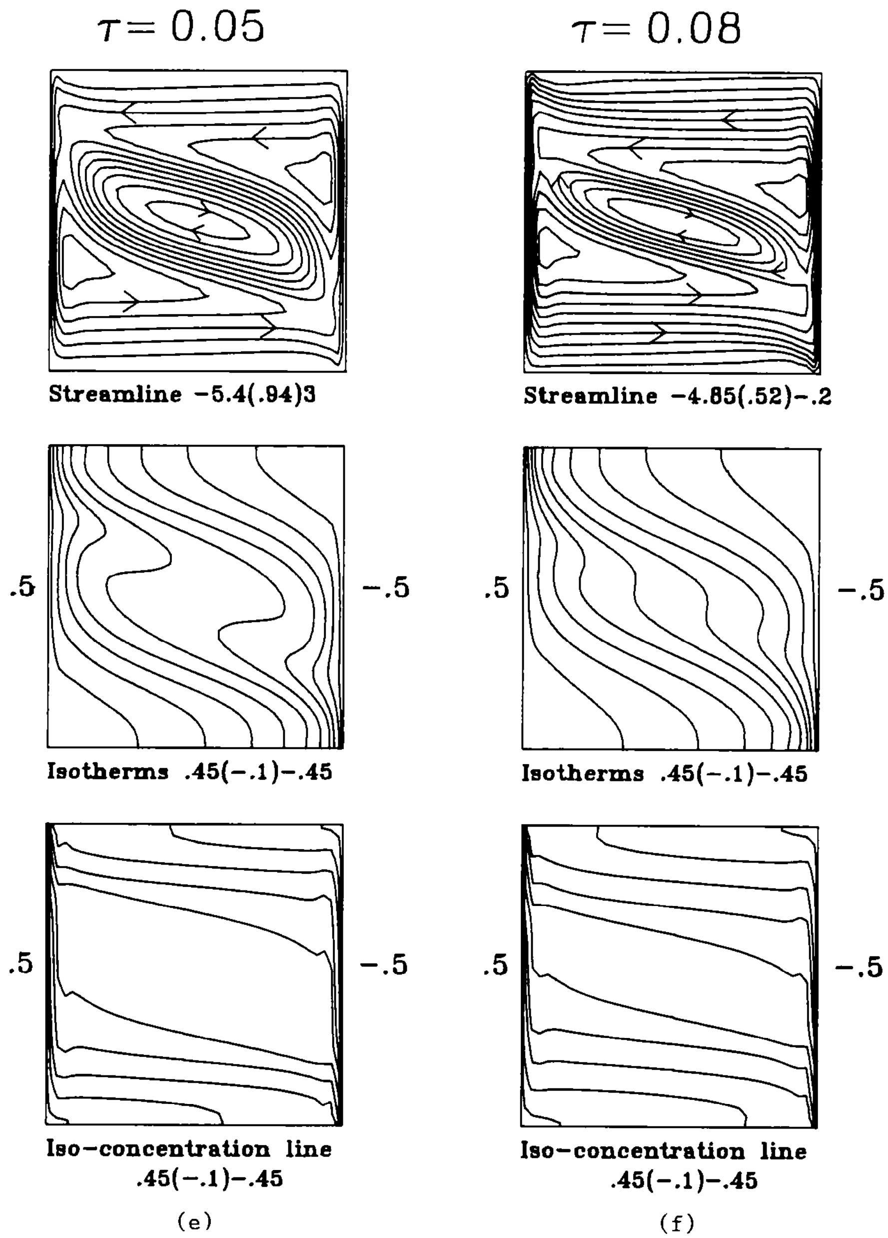

FIG. 2—*Continued.*

4. RESULTS AND DISCUSSION

The foregoing analysis indicates that the thermosolutal convection in a square enclosure is governed by five nondimensional groups—the Prandtl number Pr, thermal Grashof number Gr_t, Lewis number Le, buoyancy ratio N, and concentration ratio Γ. While computations can be carried out for any combination of these parameters, the objective here is to present a sample of results to illustrate the effects of these parameters on the cell formation processes and heat and mass transfer characteristics. In particular, we focus on the convection in a liquid–water mixture ($Pr = 7.6$) with the solutal buoyancy dominant over the thermal buoyancy ($|N| > 1$). In the actual computations Le is varied from 10 to 100, Gr_t from 10^3 to 10^5, N from -5 to -15, and Γ from 10 to 50.

4.1. *Results for* $Le = 10$

The transient development of the flow, temperature and concentration fields is illustrated in Fig. 2 for a typical case with $Pr = 7.6$, $Le = 10$, $Gr_t = 10^5$, $N = -5$ and $\Gamma = 50$ in terms of streamlines, isotherms and iso-concentration lines at selected time instants. These results indicate that initially at small τ, a uniform flow from the high concentration wall at the left to the low concentration wall at the right is induced by the high interface velocities at these walls because of the high concentration gradients existing there immediately after the sudden changes in wall concentrations. Later, the thermal buoyancy starts to exhibit some influences. Then the upward thermal buoyancy near the left wall and the downward thermal buoyancy near the right wall result in the cellular flow pattern at $\tau = 0.0003$ (Fig. 2(b)) with a primary cell moving clockwise along the cavity walls and two secondary cells contained within it. Close inspection of the isotherms and iso-concentration lines in Fig. 2(b) reveals that the temperature field develops at a faster rate since the Lewis number is much larger than unity ($Le = 10$). In fact, at $\tau = 0.0003$ the high and low concentration fluids at the vertical walls have not diffused into the fluid in the cavity. Besides, in the initial transient ($\tau \leqslant 0.0003$) all the isotherms and iso-concentration lines are parallel with the vertical walls, suggesting that the heat and mass transfer in the flow is diffusion-dominant because flow is at a low velocity in this period. At a larger τ the mass diffusion begins to show profound effects. Figure 2(c) shows that a highly elongated cell driven by the downward solutal buoyancy is formed adjacent to the left wall. Similarly, adjacent to the right wall another analogous cell is formed. These solutally driven cells gradually grow and squeeze the original cells driven by the thermal buoyancy. As time proceeds, mass diffusion continues and the solutally driven cells protrude towards the opposite walls, and the thermally driven cells shrink further, as evident from the results in Figs. 2(d) and (e). These complex flow patterns result in a significant distortion in the isotherms. Note that the secondary cells induced by the thermal buoyancy disappear when the mass diffusion driven cells grow to a certain degree (Figs. 2(e) and (f)). The thermally driven cells finally disappear at a larger τ and the flow is mainly driven by the solutal buoyancy. Based on the above observation, it can be stated that the multilayer flow structure of the double-diffusive convection for this case only exists over a certain period during the entire flow evolution. Examining the steady isotherms and iso-concentration lines dictates that heat transfer in the flow is poor and stable solutal stratification appears in the core region.

A unique feature of the natural convection driven by the combined buoyancy forces is the presence of the interface velocity at the vertical walls due to the existence of the concentration gradients there. Figure 3 presents the distributions of the interface velocity along the right wall for several time instants for the typical case. At small τ the interface velocity is nearly uniform. Later, the interface velocity becomes larger in the lower portion of the wall due to the larger concentration gradient there. A similar situation is observed for the interface velocity at the left vertical wall. The unsteady distributions of the horizontal velocity along a vertical plane right between the vertical walls ($Y = 0.5$) are shown in Fig. 4. The results clearly suggest that the flow accelerates in the initial period

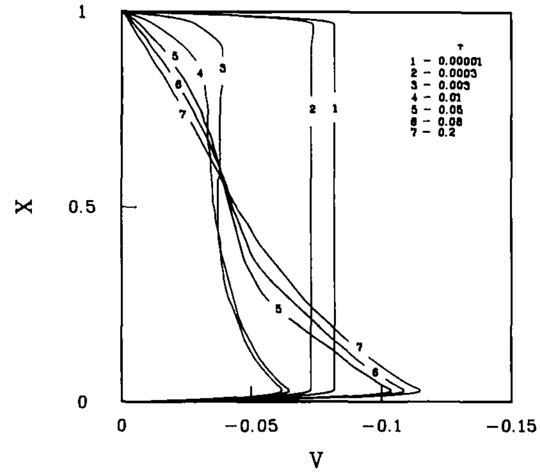

FIG. 3. Transient distributions of the interfacial velocity along the right wall for $Pr = 7.6$, $Le = 10$, $Gr_t = 10^5$, $N = -5$ and $\Gamma = 50$.

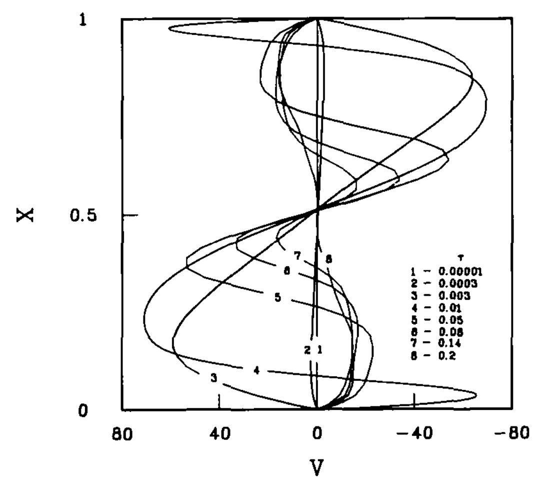

FIG. 4. Transient horizontal velocity profiles at $Y = 0.5$ for $Pr = 7.6$, $Le = 10$, $Gr_t = 10^5$, $N = -5$ and $\Gamma = 50$.

up to $\tau = 0.01$ attaining a maximum velocity. The appearance of the solutally-driven cells for $\tau \geqslant 0.01$ and the disappearance of the thermally driven cells for $\tau \geqslant 0.2$ are clearly noted. A similar phenomenon is seen for the vertical velocity distributions along a horizontal plane at the mid-height of the enclosure.

The time variations of the velocity components at selected locations indicate that substantial changes in the flow occur for $\tau < 0.03$. The temperature and concentration changes with time are rather mild. The unsteady variations of the average Nusselt and Sherwood numbers show that $\overline{Sh}$ is much larger than $\overline{Nu}$. Substantial decreases in $\overline{Nu}$ and $\overline{Sh}$ take place at small τ.

4.2. *Results for* $Le = 100$

As the Lewis number is raised to 100, the double-diffusive nature of the thermosolutal convection is

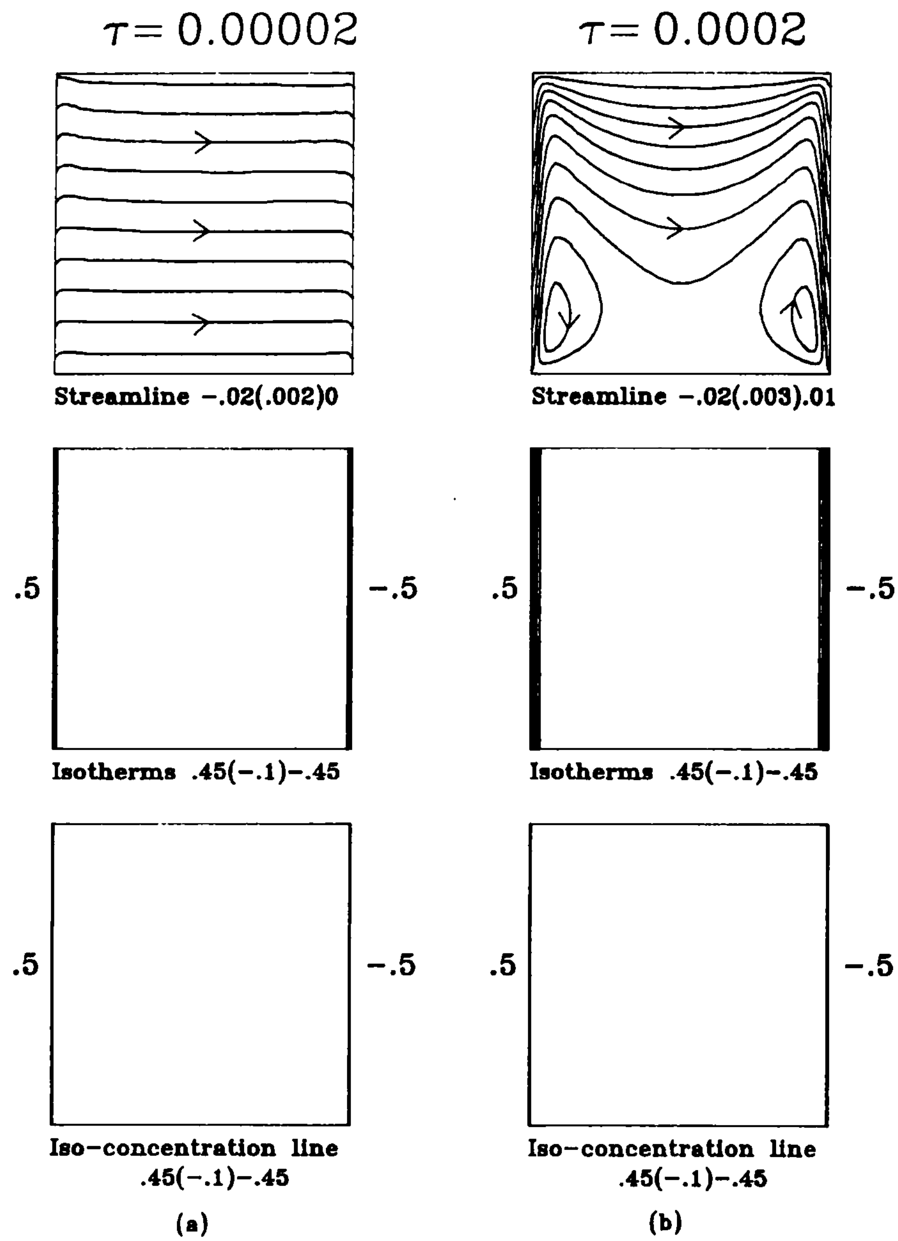

FIG. 5. Time evolution of flow patterns, isotherms and iso-concentration lines for $Pr = 7.6$, $Le = 100$, $Gr_t = 10^3$, $N = -5$ and $\Gamma = 50$ at (a) $\tau = 0.00002$, (b) $\tau = 0.0002$, (c) $\tau = 0.05$, (d) $\tau = 0.1$, (e) $\tau = 0.2$, (f) $\tau = 0.6$.

more pronounced. First, we examine low Grashof number thermosolutal convection with $Le = 100$. Figure 5 illustrates the flow formation processes and the associated temperature and concentration fields for $Gr_t = 10^3$ and $N = -5$. Again, immediately after the transient is initiated the flow is driven by the horizontal interface velocities at the side walls resulting in a horizontal left to right flow field (Fig. 5(a)). Later, the effects of thermal buoyancy set off. The upward thermal buoyancy near the left wall and the downward thermal buoyancy near the right wall greatly distort the velocity field. A pair of recirculating cells appears near the bottom corners (Fig. 5(b)). Up to $\tau = 0.02$, the flow is mainly driven by the thermal buoyancy since the concentration gradients are still confined in regions relatively close to the side walls. The solutal buoyancy begins to exert important effects at $\tau = 0.05$ outside the thermally driven cell. Figure 5(c) shows that four cells are induced in the corner regions, one at each corner. With the continuing action of the solutal buoyancy on the flow near the side walls as τ increases, the cells near the top left and bottom right corners grow. Meanwhile, the cell induced by the thermal buoyancy in the core region dwindles. In fact,

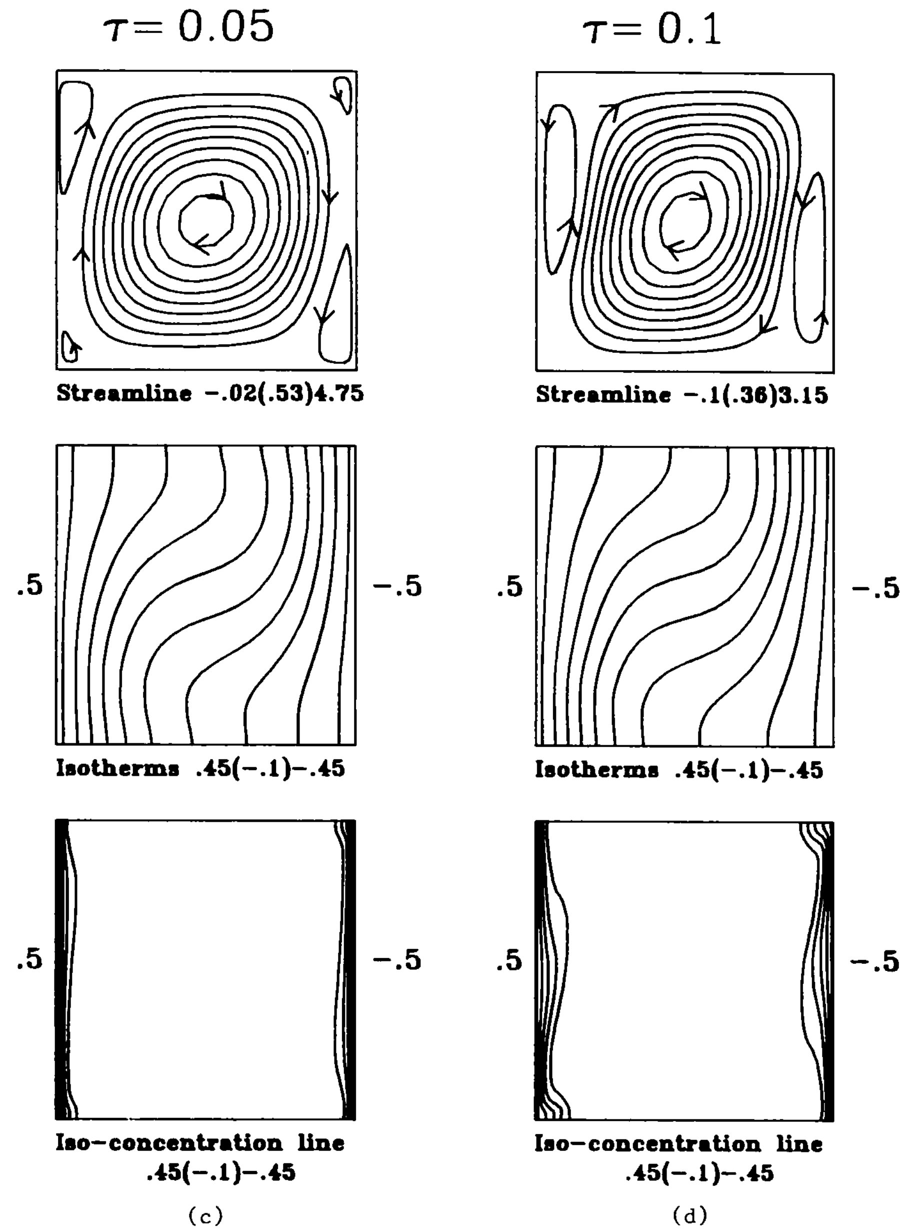

FIG. 5—*Continued.*

at $\tau = 0.6$ the enclosure is mainly occupied by the solutally induced cells. It is of interest to note in Fig. 5(f) that the solutal buoyancy is strong enough to induce a primary cell circulating along the entire enclosure walls.

The effects of the Grashof number are now discussed. The flow formation and the associated temperature and concentration development for $Gr_t = 10^5$ and $N = -5$ are presented in Fig. 6. Note that at this higher Gr_t the solutal Grashof number is also higher because $Gr_s = Gr_t \cdot N$. As the results for $Gr_t = 10^3$, the flow at $Gr_t = 10^5$ is initially driven by the horizontal interface velocities at the side walls and then by the thermal buoyancy. The results in Fig. 6, when contrasted with those in Fig. 5, indicate that raising the thermal Grashof number causes an earlier appearance of the solutally driven cells (Fig. 6(a)). Furthermore, the thermally driven cell moving clockwisely in the core region is squeezed to a small size by the solutally driven cells moving counterclockwisely. Due to the opposing thermal and solutal buoyancies, the thermal and solutal-driven cells are counterrotating. To balance these counterrotating cells, secondary cells are formed, one above and one below

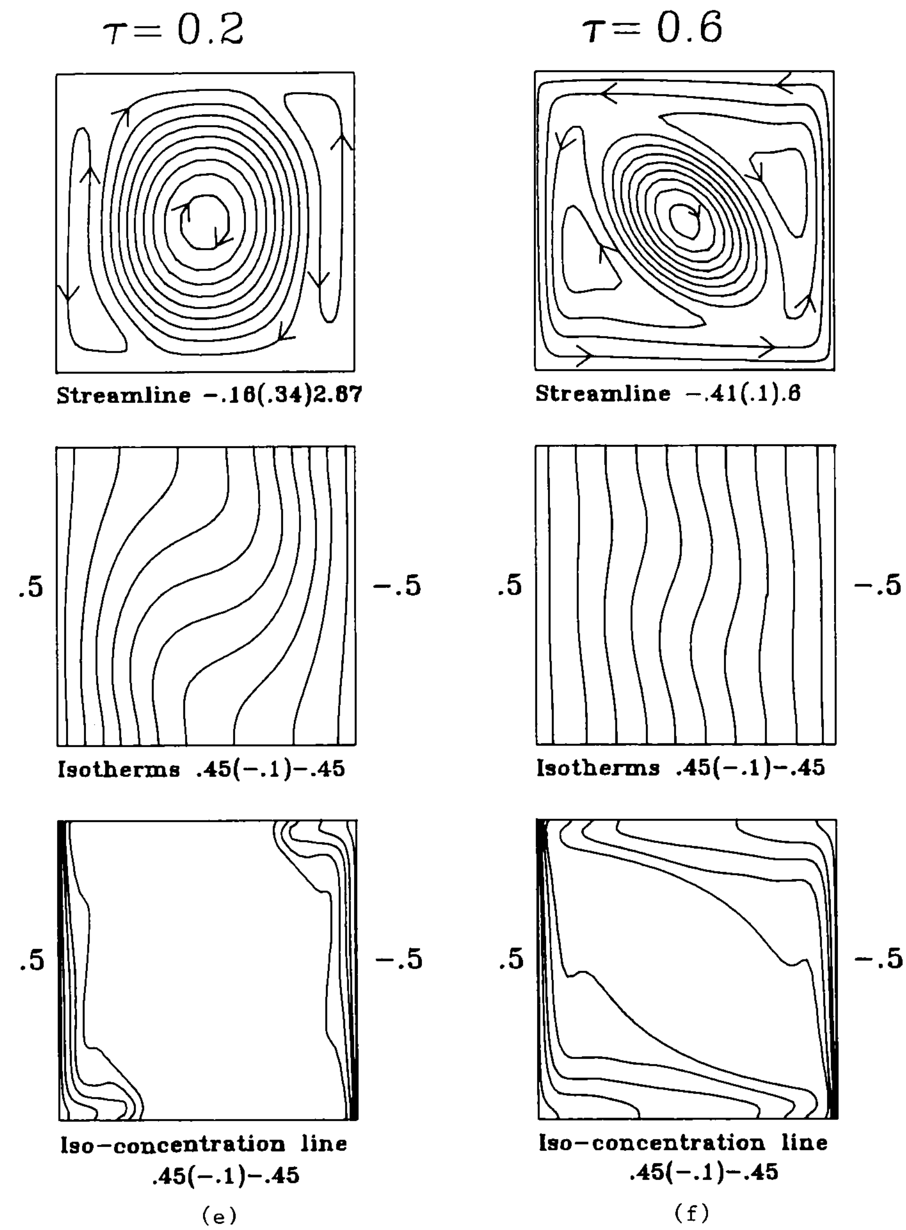

FIG. 5—*Continued.*

the thermally driven cell (Fig. 6(d)). The multilayer flow structure is thus produced by these complicated thermal–solutal interactions.

The counterrotating flow induced by the opposing buoyancies at a high Lewis number fluid is prone to instability. This is termed as the thermosolutal instability by Jiang *et al.* [21]. In fact, at $Gr_t = 10^5$ the flow clearly shows some weak unstable phenomenon, as is clear from the time variations of the horizontal and vertical velocities at a location inside the solutal boundary layer near the left wall shown in Fig. 7. Significant fluctuation is noted for the velocity component normal to the wall. The temperature and concentration variations with time given in Fig. 8 show little fluctuation except in the initial stage at small τ, so are the variations of the average Nusselt and Sherwood numbers (Fig. 9). As the Grashof numbers are further raised, significant fluctuations in U, V, T and W will result. Fluctuating characteristics in high Grashof number flow with $Le = 100$ will be the topics in the second part of this article.

According to equations (7b) and (7c), the concentration ratio Γ affects the interface velocities, which in turn influences the transport processes in the flow. Examining the results obtained in a separate computation for the transient hydrodynamic, thermal

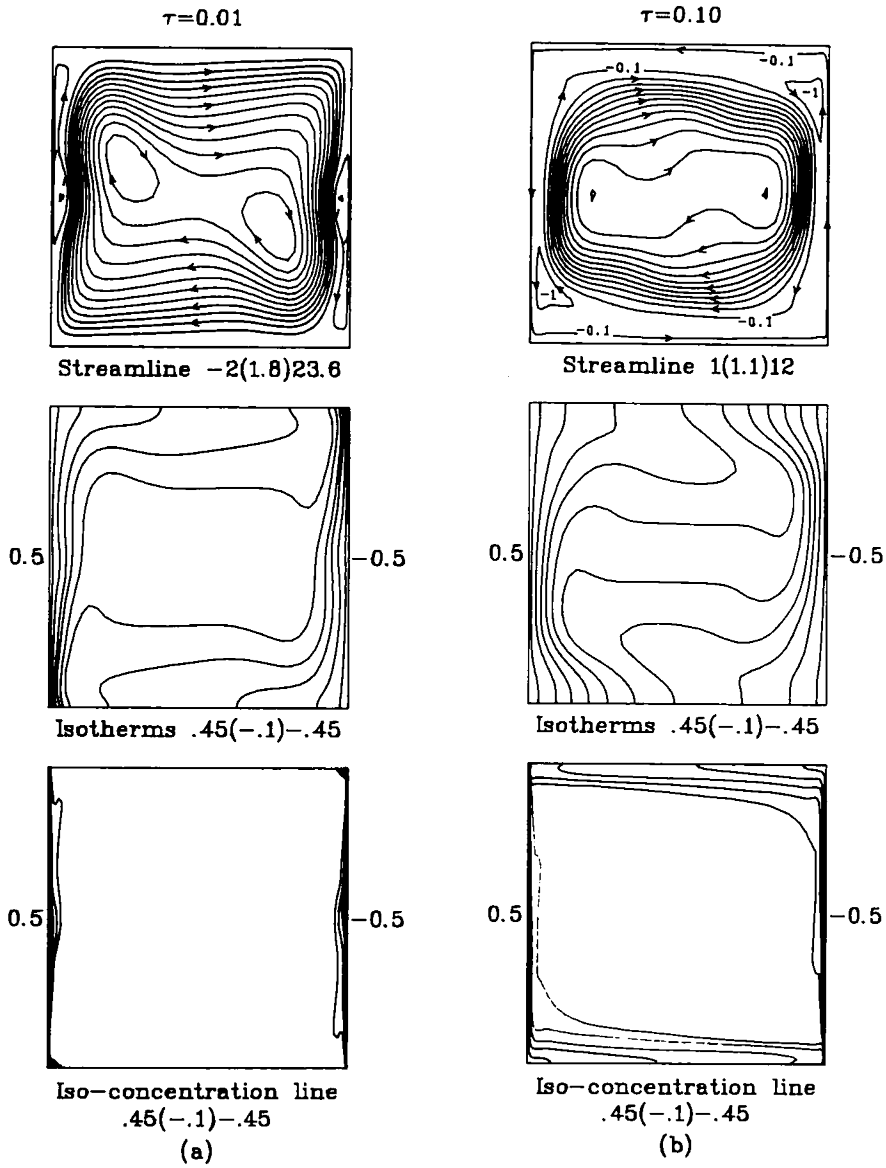

FIG. 6. Time evolution of flow patterns, isotherms and iso-concentration lines for $Pr = 7.6$, $Le = 100$, $Gr_t = 10^5$, $N = -5$ and $\Gamma = 50$ at (a) $\tau = 0.01$, (b) $\tau = 0.1$, (c) $\tau = 0.2$, (d) $\tau = 0.9$.

and solutal development for a lower concentration ratio of $\Gamma = 10$ and at $Gr_t = 10^5$, we noted that at the lower concentration ratio the interface velocities are larger, causing a delay in the first appearance of the cellular flow. The larger interface velocities is found to influence the flow near the vertical walls during the initial transient ($\tau < 0.002$). Away from the vertical walls and after the initial transient, the effects of Γ are unnoticeable.

The predicted time evolution of velocity, temperature and concentration fields for a higher buoyancy ratio of $N = -15$ and with $Gr_t = 10^5$ indicates that in the initial period ($\tau \leqslant 0.002$) a raise in N from -5 to -15 has little effect since at this small τ the concentration gradient remains confined in an extremely thin region adjacent to the vertical walls, irrespective of the magnitude of N. Later, we note that the recirculating flow induced by the solutal buoyancy appears earlier for the case with $N = -15$ and the thermally driven cell is squeezed to a smaller size. Like the increase in the Grashof number, a rise in the buoyancy ratio results in more nonuniform and higher interface velocities. Also, the changes in the velocity profiles are more significant and a higher Sherwood number results.

4.3. *Heat and mass transfer coefficients*

Variations of heat and mass transfer coefficients with the governing nondimensional groups are important in the design of heat and mass transfer equip-

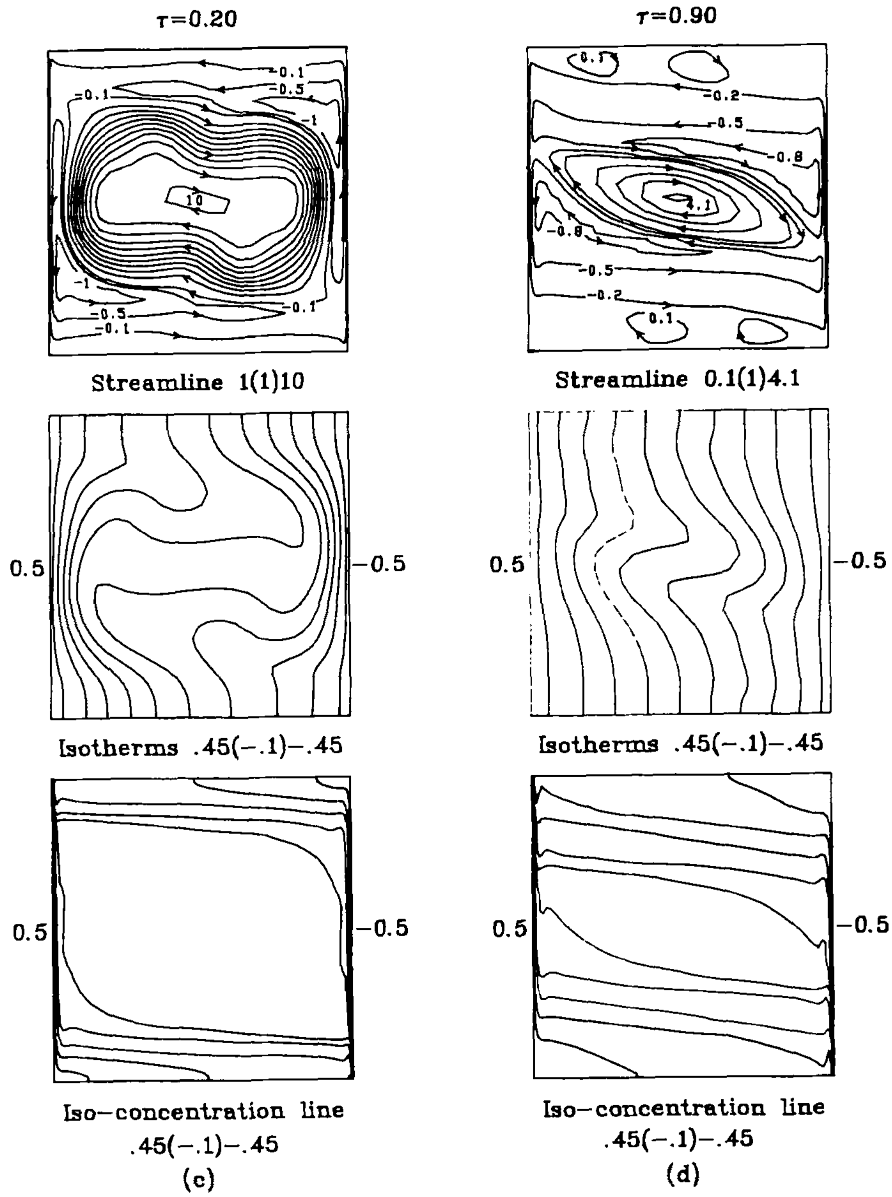

FIG. 6—*Continued.*

ments. The predicted steady average Nusselt and Sherwood numbers for various cases chosen in this study indicate that for $Le = 1$, $\overline{Nu}$ is equal to $\overline{Sh}$ and both increase with Gr_t. For fixed Gr_t, N and Γ, $\overline{Nu}$ decreases with an increase in Le, while the reverse is the case for $\overline{Sh}$. For $Le = 100$, $\overline{Nu}$ is smaller than $\overline{Sh}$ and both increase with Gr_t. A decrease in Γ causes a higher $\overline{Nu}$ but a lower $\overline{Sh}$. $\overline{Nu}$ is lower but $\overline{Sh}$ is higher for a larger buoyancy ratio. These complex relations between the $\overline{Nu}$ and $\overline{Sh}$ and the governing non-dimensional groups for $Le = 100$ apparently result from the complex flow patterns discussed above. The following empirical correlations are proposed to correlate the results:

$$\overline{Nu} = 0.112[0.993\ln^2(Le) - 6.829\ln(Le) + 13.606]Gr_t^{0.3}|N|^{-0.8} \quad (19)$$

and

$$\overline{Sh} = 0.011[0.0001112Le^3 - 0.0197Le^2 + 1.1493Le + 12.9]Gr_t^{0.285}|N|^{0.8}. \quad (20)$$

5. CONCLUDING REMARKS

Through a detailed numerical simulation of the transient thermosolutal convection in a square cavity particularly for a high Lewis number liquid–water mixture, some special features of the velocity, tem-

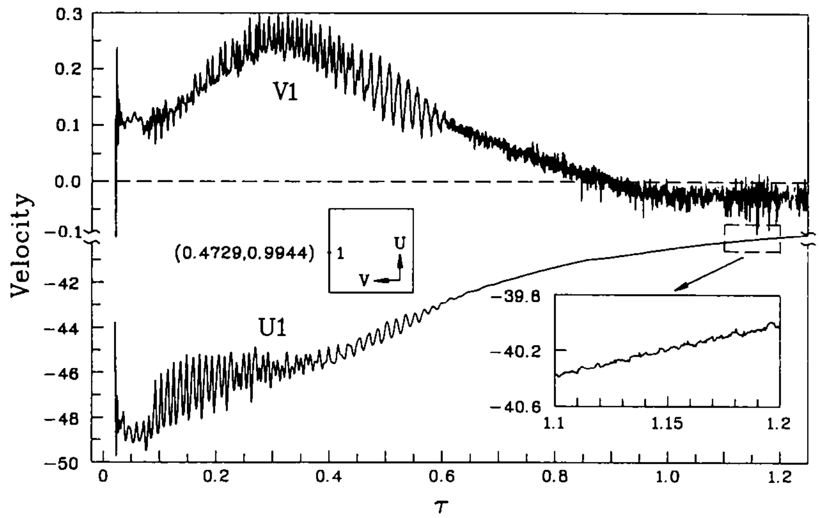

FIG. 7. Time history of U and V at the location $(X, Y) = (0.4729, 0.9944)$ for $Pr = 7.6$, $Le = 100$, $Gr_t = 10^5$, $N = -5$ and $\Gamma = 50$.

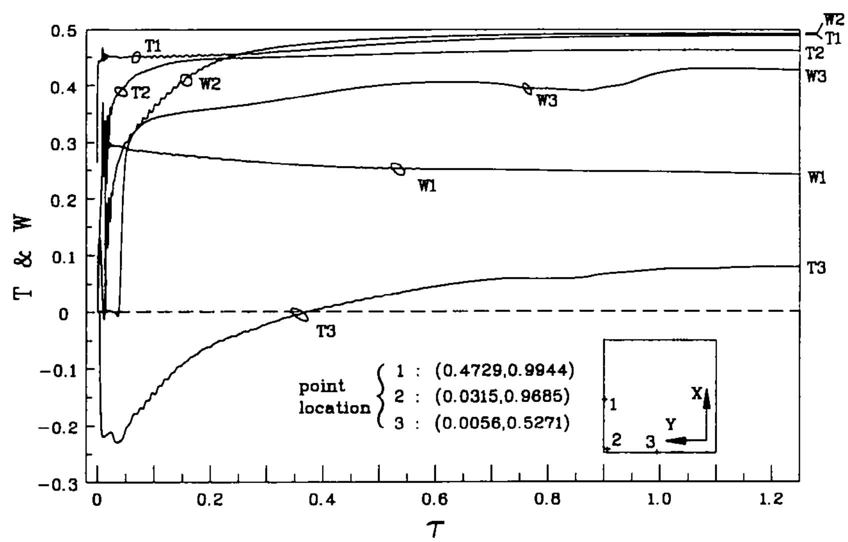

FIG. 8. Time history of T and W at the locations 1, 2 and 3 for $Pr = 7.6$, $Le = 100$, $Gr_t = 10^5$, $N = -5$ and $\Gamma = 50$.

perature and concentration development and the associated heat and mass transfer characteristics are unveiled. In a high Lewis number fluid subject to the opposing buoyancies considered here, the flow is first driven by the interface velocities and then by the thermal buoyancy up to a certain period. After that, the solutal buoyancy induces new recirculating cells near the vertical walls. With a further increase in time these solutally driven cells grow and squeeze the thermally driven cells. At $Le = 100$, a multilayer flow structure is formed. These complex flow evolutions clearly exhibit the double-diffusive nature of the buoyancy driven flow in a high Lewis number fluid.

Significant velocity, temperature and concentration variations with time appear also in a high Lewis number fluid at a high Grashof number. A further increase in the Lewis or Grashof number may lead to the flow bifurcation and the flow may become three-dimensional. Further research is needed in this area.

Natural convective transfer processes in an enclosure are sensitive to the geometry of the enclosure. An

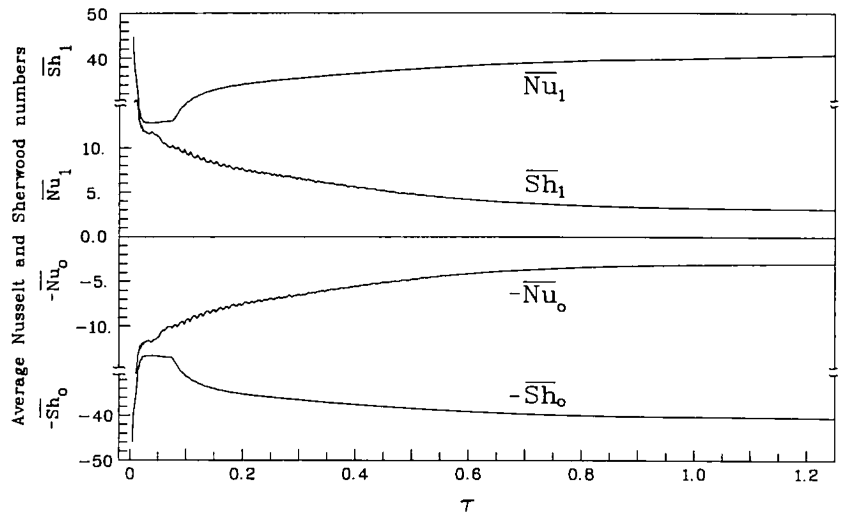

FIG. 9. Time history of average Nusselt and Sherwood numbers at $Y = 0$ and $Y = 1$ for $Pr = 7.6$, $Le = 100$, $Gr_t = 10^5$, $N = -5$ and $\Gamma = 50$.

extension of the present study to shallow and tall enclosures is of interest.

Acknowledgement—The support of this study by the engineering division of the National Science Council of Taiwan, R.O.C., through the contract NSC-77-0401-E009-10 is greatly acknowledged.

REFERENCES

1. S. Ostrach, Fluid mechanics in crystal growth—The 1982 Freeman Scholar Lecture, *J. Fluids Engng* **105,** 5–20 (1983).
2. M. Pimputkar and S. Ostrach, Convective effects in crystals grown from melt, *J. Crystal Growth* **55,** 614–646 (1981).
3. W. E. Langlois, Buoyancy-driven flows in crystal-growth from melts, *Ann. Rev. Fluid Mech.* **17,** 191–215 (1985).
4. F. Rosenberger, Fluid mechanics in crystal growth from vapors, *PCH Physico-Chem. Hydrodyn.* **1,** 3–26 (1980).
5. B. S. Jhaveri and F. Rosenberger, Expansive convection in vapor transport across horizontal rectangular enclosures, *J. Crystal Growth* **57,** 57–64 (1982).
6. B. L. Markham and F. Rosenberger, Diffusive-convective vapor transport across horizontal rectangular enclosures, *J. Crystal Growth* **67,** 214–254 (1984).
7. S. Ostrach, Natural convection with combined buoyancy forces, *PCH Physico-Chem. Hydrodyn.* **1,** 233–247 (1980).
8. Y. Kamotani, L. W. Wang, S. Ostrach and D. H. Jiang, Experimental study of natural convection in shallow enclosures with horizontal temperature and concentration gradients, *Int. J. Heat Mass Transfer* **28,** 165–173 (1985).
9. S. Ostrach, H. D. Jiang and Y. Kamotani, Thermosolutal convection in shallow enclosures, *ASME–JSME Thermal Engng Joint Conf.*, Hawaii, U.S.A. (1987).
10. J. Lee and M. T. Hyun, Experimental study of natural convection due to combined buoyancy in a low-aspect ratio enclosure, *ASME–JSME Thermal Engng Joint Conf.*, Hawaii, U.S.A. (1987).
11. L. W. Wang and P. C. Chuang, Flow patterns of natural convection in enclosures with horizontal temperature and concentration gradients, *Proc. 8th Int. Heat Transfer Conf.*, San Francisco, California, U.S.A., Vol. 4, pp. 1477–1481 (1986).
12. L. W. Wang, J. J. Chen and C. T. Chen, Fingering flow patterns of thermosolutal convection in rectangular enclosures, *Proc. National Fluid Dynamics Congress*, AIAA, ASME, ASCE, SIAM, and APS, Cincinnati, Ohio, 24–28 July (1988).
13. P. Ranganathan and R. Viskanta, Natural convection in a binary gas in rectangular cavities, *ASME–JSME Thermal Engng Joint Conf.*, Hawaii, U.S.A. (1987).
14. H. Han and T. H. Kuehn, A numerical simulation of double-diffusive natural convection in a vertical rectangular enclosure, *National Heat Transfer Conf., Heat Transfer in Convective Flows*, HTD 107, pp. 149–154 (1989).
15. C. Benard, D. Gobin and J. Thevenin, Thermosolutal natural convection in a rectangular enclosure: numerical results, *National Heat Transfer Conf., Heat Transfer in Convective Flows*, HTD-107, pp. 249–254 (1989).
16. O. V. Trevisan and A. Bejan, Combined heat and mass transfer by natural convection in a vertical enclosure, *J. Heat Transfer* **109,** 104–112 (1987).
17. J. M. Hyun and J. W. Lee, Double-diffusive convection in a rectangle with co-operating horizontal gradients of temperature and concentration, *Int. J. Heat Mass Transfer* **33,** 1605–1617 (1990).
18. J. W. Lee and J. M. Hyun, Double-diffusive convection in a rectangle with opposing horizontal temperature and concentration gradients, *Int. J. Heat Mass Transfer* **33,** 1619–1632 (1990).
19. R. Krishnan, A numerical study of the instability of double-diffusive convection in a square enclosure with horizontal temperature and concentration gradients, *National Heat Transfer Conf., Heat Transfer in Convective Flows*, HTD 107, pp. 357–368 (1989).
20. A. Bejan, Mass and heat transfer by natural convection in a vertical cavity, *Int. J. Heat Fluid Flow* **6,** 149–159 (1985).
21. H. D. Jiang, S. Ostrach and Y. Kamotani, Thermosolutal convection with opposed buoyancy forces in shallow enclosures, *ASME HTD* **99,** 53–66 (1988).
22. T. F. Lin, C. C. Huang and T. S. Chang, Transient binary mixture natural convection in square enclosures, *Int. J. Heat Mass Transfer* **33,** 287–299 (1990).
23. S. G. Schladow, J. C. Patterson and R. L. Street, Transient flow in a side-heated cavity at high Rayleigh number: a numerical study, *J. Fluid Mech.* **200,** 121–148 (1989).
24. S. Paolucci and D. R. Chenoweth, Transition to chaos

in a differentially heated vertical cavity, *J. Fluid Mech.* **201,** 379–410 (1989).
25. A. Bejan, *Convection Heat Transfer*, Chap. 9, pp. 91–104. Wiley, New York (1983).
26. F. Rosenberger and G. Muller, Interfacial transport in crystal growth, a parametric comparison of convective effects, *J. Crystal Growth* **65,** 91–104 (1983).
27. F. Rosenberger, *Fundamentals of Crystal Growth* **I,** Chap. 5, pp. 215–391. Springer, New York (1979).
28. A. J. Chorin, Numerical solution of the Navier–Stokes equations, *Math. Comput.* **22,** 745–762 (1968).
29. R. Temam, On an approximate solution of the Navier–Stokes equations by the method of fractional step: Part 1, *Arch. Ration. Mech. Analysis* **32,** 135–153 (1969).
30. T. Kawamura, H. Takami and K. Kuwahara, New higher-order upwind scheme for incompressible Navier–Stokes equations, *Proc. 9th ICNMFD*. Springer (1985).
31. D. A. Anderson, J. C. Tannehill and R. H. Pletcher, *Computational Fluid Mechanics and Heat Transfer*, p. 75 and Chap. 5, pp. 181–255. Hemisphere/McGraw-Hill, New York (1984).
32. K. de Rivas, On the use of nonuniform grids in finite-difference equations, *J. Comp. Phys.* **10,** 202–210 (1972).
33. G. E. Schneider and M. Zedan, A modified strongly implicit procedure for the numerical solution of field problems, *Numer. Heat Transfer* **4,** 1–19 (1981).
34. G. de Vahl Davis, Natural convection of air in a square cavity: a bench mark numerical solution, *Int. J. Numer. Meth. Fluids* **3,** 249–264 (1983).
35. D. R. Chenoweth and S. Paolucci, Natural convection in an enclosed vertical air layer with large horizontal temperature differences, *J. Fluid Mech.* **160,** 173–210 (1986).
36. J. C. Patterson and S. W. Armfield, Transient feature of natural convection in a cavity, *J. Fluid Mech.* **219,** 469–497 (1990).